Structural and electrical properties of $Li_2AlMn_3O_8$

Wan Masku Wan Mohamed [1,2], *Rozana Aina* Maulat Osman [1,3], *Mohd Sobri* Idris [1,2] *and Nazuhusna* Khalid [3] *and Nurul Izza* Mohd Nor[3]

[1]Centre for Frontier Materials Research, Universiti Malaysia Perlis, 01000 Kangar, Perlis, Malaysia.
[2]School of Materials Engineering, Universiti Malaysia Perlis, Jejawi, 02600 Arau, Perlis, Malaysia.
[3]School of Microelectronic Engineering, Universiti Malaysia Perlis, Pauh Putra, 02600 Arau, Perlis, Malaysia.

Abstract. The spinel $Li_2AlMn_3O_8$ was synthesized using a conventional solid-state method at 800°C for 12 h in air. The samples were analyzed using X-ray Diffraction (XRD) and Electrochemical Impedance Analyzer to study the structural and electrical properties of the samples. Well defined reflections were obtained with additional weak peaks of Al_2O_3. However, small values of χ^2 indicating a good agreement between calculated and observed pattern. A single semicircle from the complex plane plot (Z" vs. Z'), and the capacitance value at the top point of semicircular arc was determined as a grain boundary region. The conductivity of $Li_2AlMn_3O_8$ at room temperature is about 2.99 x 10^{-5} S cm^{-1}. Meanwhile, the Arrhenius plot related from conductivity shows the activation energy also fairly similar at frequency range from 10^1 to 10^5 Hz.

1 Introduction

Lithium ion batteries (LIB) have been widely used in electronic products in the past decade. Inexpensive and environmentally benign spinel cubic structure of $LiMn_2O_4$ has Fd3m symmetry in which the Li^+ and the Mn^{3+}/Mn^{4+} are located in the 8a tetrahedral and 16d octahedral sites, respectively while O^{2-} ions was occupy the 32e sites. The 8a sites share a face with the vacant 16c octahedral sites, offers 3D conduction pathways for Li^+ ions .[1]

However, this composition has a bottleneck related to capacity fades issues on charge-discharge cycling. Widespread studies have been focused towards various strategies to improve the cycleability of $LiMn_2O_4$. Among these, one effective approach is to substitute small amount of dopant ions place of Mn ions. It is believed that, the structure of $LiMn_2O_4$ become more stable since the dopant ions are occupied in the 16d sites of the Mn ions in the spinel lattice.[2]

The substitution of aluminium as a non-transition metal in $LiMn_2O_4$ has a potential of reducing strain during repeated cycling and facilitates a higher discharge capacity retention.[3] In this paper, the studied of the new composition of spinel structure, $Li_2AlMn_3O_8$ was reported. Much attention has been done to investigate the effect of non-transition metal that has fixed oxidation state in the 16d site of the spinel structure. Result of the structural and electrical property of $Li_2AlMn_3O_8$ was reported. The structural property has been done using XRD, coupled with Rietveld refinement. Meanwhile, to meet the needs of analyzing the electrical properties of $Li_2AlMn_3O_8$, electrochemical impedance analyzer has been used. The electrical properties was discussed with a set of impedance data measured between 303K and 26K.

2 Experimental

$Li_2CoMn_3O_8$, $Li_2NiMn_3O_8$, and $Li_2AlMn_3O_8$ samples were prepared by the conventional solid-state. Reagent grade $Li(CH_3COO)\cdot 2H_2O$, $Al(NO_3)_3\cdot 9H_2O$ and $Mn(CH_3COO)_2\cdot 4H_2O$ were used as raw materials. The powder samples from conventional solid state synthesis were prepared using a stoichiometric amount of raw materials were mixed and ground by using pestle and mortar. After that, the samples were slowly heated to remove acetates at 400°C for 12 h. Then, samples were further heated at 800°C for 12 h in the air with intermittent grinding.

Bruker D2 Phaser benchtop X-ray diffractometer equipped with LYNXEYE 1D-detector with Cu–Kα radiation) was used to analyzed the purity of the final products at room temperature with a scan rate about 1.0 s/step and 0.02 of step size. The detector is the fast detector with 192 silicon strips. Rietveld refinements were carried out by using GSAS/EXPGUI software to determine the structural parameters.

For electrical measurements, a pellet was cold-pressed uniaxially at 4 tons, sintered at 950°C for 12 hours in order to increase the mechanical strength, slowly cooled to 600°C and maintained at 600°C for 12 hours before slowly cooled to room temperature. In/Ga paste electrodes were coated on opposites sides of sintered pellet. Impedance measurements were carried out over the frequency range 10 Hz-100 kHz, using

* Corresponding author: author@e-mail.org

Hioki Impedance Analyzer IM3570 at the temperature range between 303K and 268K.

3 Results and Discussion

The powder XRD pattern for $Li_2AlMn_3O_8$ that were prepared at 800 °C in air was shown in Fig. 1. The XRD pattern of $Li_2AlMn_3O_8$ shows very well defined reflections; refer to PDF Card 00-048-0261. All the peaks indexable in the Fd-3m space group with a cubic lattice. The lattice belongs to face-centered cubic, since the planes agreed with rule for reflection to be observed, which (h, k, l) either all odd or all even. However, a few extra peaks could be observed at 2θ=37.49°, 45.65° and 66.50°, indicating the presence of mixed phases. The additional peaks in these diffractogram are ascribed to Al_2O_3.

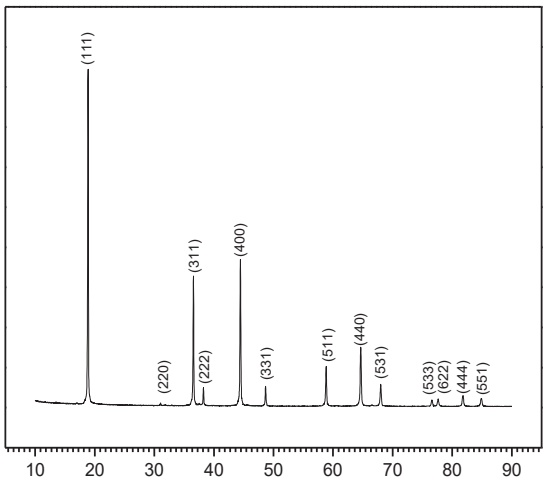

Fig. 1. XRD pattern of $Li_2AlMn_3O_8$ heated in air at 800°C for 12 h.

Replacing the transition metal with Al is not easy. It was reported that, at calcination temperatures above 600 °C, the inessential phases such as Al_2O_3, β-$LiAlO_2$ and γ-$LiAlO_2$, can easily form.[3] Manganese was expected to become $Mn^{3+/4+}$ in the composition of $Li_2AlMn_3O_8$, since Al has fixed valence states as Al^{3+}. Al^{3+} mostly occupies in octahedral site (16d) and was predicted to stabilize the spinel structure. However, the presence of additional peaks of Al_2O_3 was indicated Mn oxidize as Mn^{4+}.

The purpose of obtaining the details of crystallographic properties of sample was accomplished with structure refinement using Rietveld analysis. The refinement were performed regarding to the steps described elsewhere.[4–6] The spinel structure of $Li_2CoMn_3O_8$ was used as the structural model with a space group Fd-3m. Li ions were located at 8a-site (0.125,0.125,0.125), transition metal ions (Al and Mn) located at 16d-site (0.5,0.5,0.5) and oxygen at the 32e-site (0.2629,0.2629,0.2629). The initial structure model assumed that there is no cation disorder between Li and transition metal ions. Thus, the occupancy of Li ion at 8a-site was fixed at 100%, while transition metals at 16d-site were fixed with Al, Mn1 and Mn2 as 0.25, 0.25 and 0.5, respectively. The detail of crystallographic properties of $Li_2AlMn_3O_8$ was summarized in Table 1.

Table 1. Refined structural data for $Li_2AlMn_3O_8$ synthesized at 800°C in air for 12 h

Composition	**$Li_2AlMn_3O_8$**
a (Å)	8.1548(1)
Volume (Å^3)	542.31(1)
Oxygen, XYZ	0.2625(1)
8a Li occ.	1.00
16d Al occ.	0.25
16d Mn occ.	0.25
16d Mn occ.	0.50
32e O occ.	1.00
8a Li U_{iso}	0.01(1)
16d Al U_{iso}	0.009(1)
16d Mn U_{iso}	0.009(1)
16d Mn U_{iso}	0.009(1)
32e O U_{iso}	0.011(1)
R_{wp}	8.42 %
R_p	6.62 %
χ^2	2.138

The disagreements between observed and calculated patterns were represented as R_{wp}, R_p, and χ^2. Small values of χ^2 indicating a good agreement between calculated and observed pattern. The small weak peaks of Al_2O_3 were excluded and negligible during the refinement.

Fig. 2 shows a set of typical impedance data measured for $Li_2AlMn_3O_8$. An impedance complex plane, which is imaginary vs. real at 303K was plot in Fig. 2(a). The value of capacitance calculated from the relation ωRC=1 at the maximum point of semicircle is 5.88 x 10^{-8} F. Meanwhile, Z", M" spectroscopic plots from the relation of Z* and M* at 303K was shown in Fig. 2(b). The plots shows Z" and M" peak at low frequencies and high frequencies, respectively. A capacitance vs. frequency plots (shown in Fig. 2(c)) shows the frequency and temperature dependence. The value of capacity was decreased with increasing the frequency, with at three orders of magnitude while decreased with decreasing of temperature between 303K and 268K. Other than that, the conductivity of $Li_2AlMn_3O_8$ also shows clearly frequency dependence as shown in Fig. 2(d). A clear plateau was observed at the intermediate measured frequency (between 10^2 and 10^3 Hz). The plot also shows temperature dependent conductivity since the conductivity was decreased with decreasing the temperature from 303K to 268K. The conductivity at room temperature is about 2.99 x 10^{-5} S cm^{-1}, while an Arrhenius plots in Fig. 2(e) shows average of activation energy at frequency between 10 Hz and 100 kHz is about 0.3 eV.

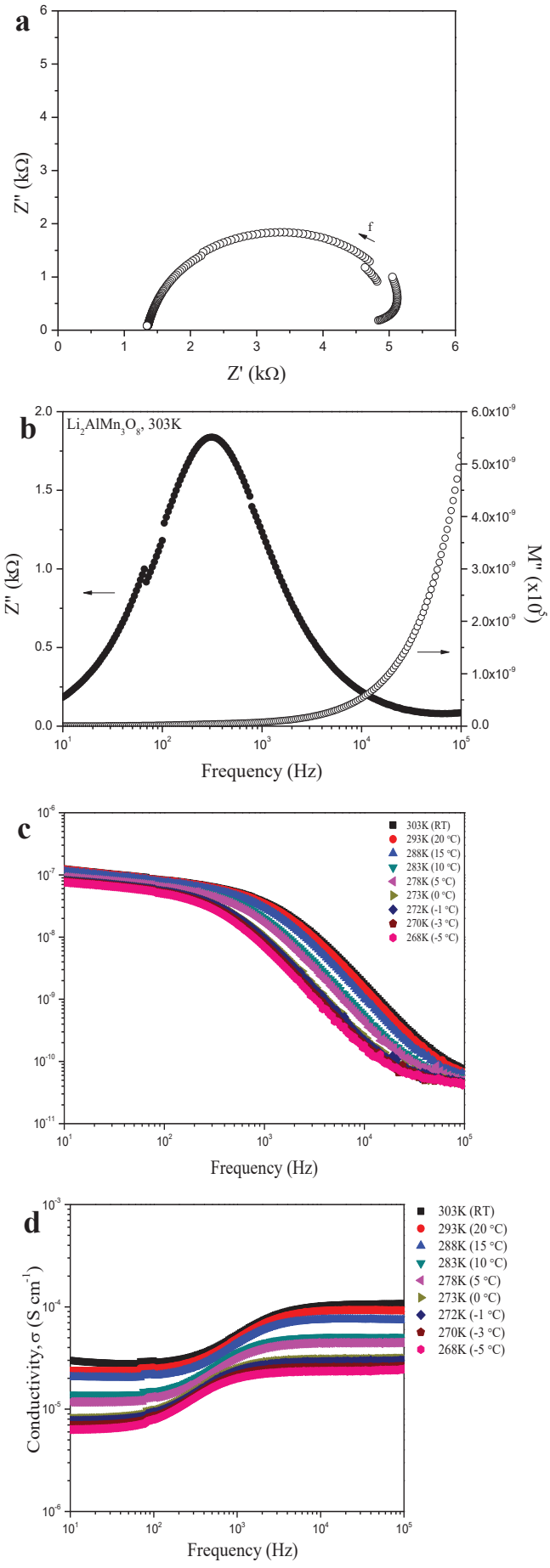

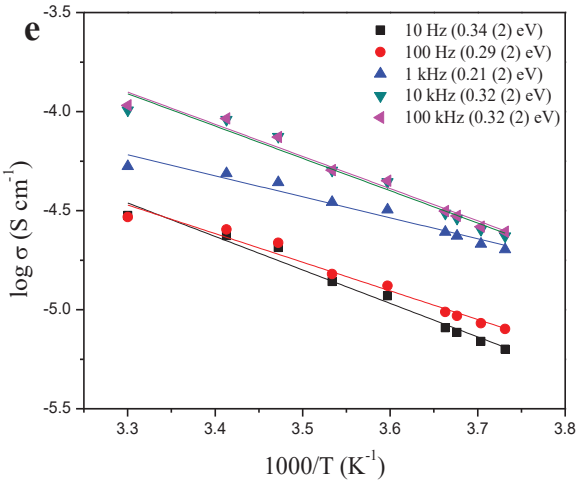

Fig. 2. Typical IS data set of $Li_2AlMn_3O_8$ (a) an impedance complex plane at 303K, (b) Z", M" spectroscopic plots at 303K, (c) capacitance spectroscopic plot, (d) conductivity spectroscopic plot and (e) Arrhenius plot.

The magnitude and direction of the complex number can be expressed by real, Z' and imaginary, Z' components through the relation;

$$Z^* = Z' - jZ'' \text{ where } j = \sqrt{-1} \quad (1)$$

From the top point of semicircular arc (Fig. 2 (a)), the capacitance value was attributed to grain boundary regions of the sample.[7] The complex electric modulus, M*, is related to the complex impedance Z*, through the relation;

$$M^* = j\omega C_o Z^* \quad (2)$$

Where $M' = \omega C_o Z''$ and $M'' = \omega C_o Z'$; $C_o = \varepsilon_o A/l$ is the vacuum capacitance of the empty measuring cell with electrode area, A and separation, l. The permittivity of free space, $\varepsilon_o = 8.854 \times 10^{-14}$ Fcm^{-1}.[8] Non-ideal RC element of $Li_2AlMn_3O_8$ also observed from the Z", M" vs. frequency plot (Fig. 2(b). The Z" spectra are broadened on the low frequency side of the peak maximum, while the M" spectra are broadened on the high frequency side. These two separated peak maxima contributed to the non-ideal RC element, with an additional parallel constant phase element (CPE). An accurate fit experimental data for a range of electrically homogeneous and heterogeneous materials also was provided by insertion of a CPE into equivalent circuits.[9,10] The frequency dependence capacitance of this composition also lies into grain boundary region. At low frequency, capacitance almost constant contributes more to grain boundary. Other than that, the capacitance was declined with increasing of frequency. The limiting high frequency capacitance corresponds to the bulk capacitance. However, the bulk capacitance was modified by the grain boundary capacitance.[10]

The electrical conductivity and lithium-ion diffusivity are most important properties responsible for the electrochemical performance of the LIB cathode material. The conductivity can be written as;

$$\sigma = 1/R*l/A \quad (3)$$

where l is the thickness and A the area of the electrode deposited on the sample. Low conductivity may lead to a poor rate capability because it provides a kinetic limitation and induces polarization during lithium intercalation and deintercalation. Using Eq. (3), the conductivity of $Li_2AlMn_3O_8$ was obtained. The plot shows frequency dependent conductivity of of $Li_2AlMn_3O_8$. The frequency dependence conductivity spectrum exhibits three different regions. The three different regions are; (a) low frequency dispersed, (b) an intermediate plateau and (c) conductivity dispersion at high frequencies. In the low and intermediate frequency region, conductivity is almost found to be frequency independent and equal to DC conductivity.[10] The intermediate frequency region is obtained due to the transportation of mobile ions response to applied electric field.[11] The intermediate frequency conductivity was clearly seen on $Li_2AlMn_3O_8$ (Fig. 2(d)), with existence of clear plateau between 10^2 and 10^3 Hz. In high-frequency region, the conductivity increases with frequency and become more sensitive. It is caused by the situation known as hopping frequency. It is shifted towards higher frequency with a rise in temperature. The conductivity increases due to long range movement of charge carriers and the material show the relaxor properties in high frequency. The difference of conductivity in the low-frequency range is due to the polarization belongings. The accumulation of charge occurs at very low frequencies, hence drop the conductivity. An Arrhenius law that was related with conductivity can be presented as;

$$\sigma = \sigma_o \exp[-E_a/kT] \quad (4)$$

where σ_o is a pre-exponential factor and characteristics of the materials, Ea, k, and T are activation energy for conduction, Boltzmann's constant and the absolute temperature, respectively.[12] The Arrhenius plot from Eq. (4) in shows the activation energy also fairly similar at frequency range from 10^1 to 10^5 Hz.

4 Conclusions

The composition of spinel $Li_2AlMn_3O_8$ was synthesized with the aim of investigates the structural and electrical properties. XRD studies shows that, this composition had existence of extra peaks belongs to Al_2O_3 at 2θ=37.49°, 45.65° and 66.50°. Meanwhile, the refinement data shows a good agreement between calculated and observed pattern. A single semicircle from the complex plane plot (Z" vs. Z'), and the capacitance value at the top point of semicircular arc was determined as a grain boundary region. Non-ideal RC element also observed from the Z", M" vs. frequency plot, with the presence of two separated peak maxima. The conductivity of $Li_2AlMn_3O_8$ at room temperature is about 2.99 x 10^{-5} S cm^{-1}. An Arrhenius plot related from conductivity shows the activation energy also fairly similar at frequency range from 10^1 to 10^5 Hz with the average about 0.3 eV.

This research was financially supported by the Fundamental Research Grant Scheme (FRGS) (Grant No.: 9003-00429) and MyBrain15 scholarship from Ministry of Higher Education Malaysia (MOHE).

References

1. M.M. Thackeray, W.I.F. David, P.G. Bruce, J.B. Goodenough, Mater. Res. Bull. **18** (1983)
2. B. Hwang, R. Santhanam, D. Liu, J. Power Sources. **101** (2001).
3. G.T. Fey, C. Lu, T.P. Kumar, Mater. Chem. Phys. **80** (2003).
4. M. Sobri Idris, a. R. West, J. Electrochem. Soc. **159** (2012).
5. T.Q. Tan, M.S. Idris, R.A.M. Osman, M.V. Reddy, B.V.R. Chowdari, Solid State Ionics. **278** (2015)
6. J.J. Biendicho, A.R. West, Solid State Ionics. **203** (2011).
7. J.T.S. Irvine, D.C. Sinclair, A.R. West, Adv. Mater. **2** (1990).
8. D.C. Sinclair, D.C. Bol. La Soc. Esp. Ceram. Y Vidr. **65** (1995).
9. J.J. Biendicho, A.R. West, Solid State Ionics. **226** (2012).
10. A.R. West, D.C. Sinclair, N. Hirose, J. Electroceramics. **1** (1997).
11. T. Badapanda, R.K. Harichandan, S.S. Nayak, A. Mishra, S. Anwar, Process. Appl. Ceram. **8** (2014).
12. S. Lanfredi, a. C.M. Rodrigues, J. Appl. Phys. **86** (1999).